Epitaxial ScAlN Etch-Stop Layers Grown by Molecular Beam Epitaxy for Selective Etching of AlN and GaN

Matthew T. Hardy, Brian P. Downey, *Member, IEEE*, David J. Meyer, *Senior Member, IEEE*, Neeraj Nepal, David F. Storm, and D. Scott Katzer, *Senior Member, IEEE*

***Abstract*—Although selective dry etches exist for GaN, it is difficult to selectively etch AlN in heterostructures with other conventional III-N epitaxial materials. The reduction in etch rate resulting from the addition of 2%–16% scandium to $Sc_xAl_{1-x}N$ in conventional $Cl_2/BCl_3/Ar$ inductively coupled plasma etching is presented. Smooth, epitaxial $Sc_xAl_{1-x}N$ layers are grown by RF-plasma-assisted molecular beam epitaxy directly on 4H-SiC substrates. The etch selectivity with respect to AlN is as high as 10.6 and 11.2 for $x = 0.02$ and 0.16, respectively, allowing $Sc_xAl_{1-x}N$ to act as an etch-stop layer with minimal misfit strain when grown within either AlN or GaN based heterostructures.**

***Index Terms*—Etch-stop layers, GaN, scandium aluminum nitride, selective etching, inductively coupled plasma, reactive ion etches, molecular beam epitaxy, HEMTs.**

I. Introduction

DEVELOPMENT of novel nitride materials compatible with conventional III-N semiconductors will expand the functionality and design space of wide bandgap semiconductors [1], [2]. $Sc_xAl_{1-x}N$ alloys have emerged as a promising new functional nitride material system which has piezoelectric and spontaneous polarization coefficients more than a factor of three higher than AlN for $x = 0.43$ [3]–[5], leading to a factor of five improvement in the piezoelectric response compared to AlN. The piezoelectric properties of ScAlN make it attractive for acoustoelectric applications such as RF resonators and various other MEMS devices [6]–[9]. High quality, epitaxial ScAlN is also a promising barrier material for high current density transistors, which can be grown lattice-matched to GaN [10]. Recently, a two-dimensional electron gas has been demonstrated in a ScAlN/GaN/AlN/GaN structure with a mobility of 910 $cm^2/V{\cdot}s$ and a sheet charge density of 3.4×10^{13} cm^{-2} [10], demonstrating the potential of ScAlN as a high-electron-mobility transistor (HEMT) barrier material. Additionally, due its wide bandgap, ScAlN is also promising for use in polarization engineered deep-UV optoelectronics [11].

In addition to modifying mechanical, electrical, and optical properties, alloying of Sc with AlN has the potential to alter the dry etch rate of the alloy [12]. Etch-stop layers (ESLs) make use of material dependent etch rates to significantly slow or stop an etch process at a specific location in a layer stack. ESLs can improve etch depth uniformity and run-to-run reproducibility while enabling precise etch depth control. An ideal ESL has a high selectivity, defined as the ratio of the surrounding material etch rate to the ESL etch rate, while also having minimal epitaxial strain and smooth surface morphology after etching, devoid of pitting or micromasking.

While several dry etch chemistries and their corresponding ESLs exist for etching GaN [13]–[15], there is no widely applied etch chemistry/ESL combination for selective etching of AlN relative to another layer. Several critical device-manufacturing steps would be enabled or improved by an AlN-compatible ESL, including improved control of AlN substrate removal for DUV light-emitting diodes (LED)s, ridge height control in laser diodes [16], and gate recess etching accuracy in high Al content InAlN- and AlN-barrier HEMTs.

In this work, we present the growth of epitaxial $Sc_xAl_{1-x}N$ layers with $x = 0.02$–0.19, and show etch rate selectivity for $Sc_xAl_{1-x}N$ ESLs relative to GaN and AlN using a standard Cl_2-based inductively coupled plasma (ICP) dry etch [17].

II. ScAlN Epitaxial Growth

While the majority of ScAlN deposition has been done using sputtering, we have recently demonstrated epitaxial growth of ScAlN using molecular beam epitaxy (MBE) [10]. For moderate Sc mole fraction $x < 0.25$, ScAlN can be grown over a range of substrate temperatures from 350–810 °C, and is limited by slight roughening at the low temperature range and Al re-evaporation for temperatures well above 810 °C. For ScAlN samples grown on GaN at a substrate temperature of 730 °C, the rms surface roughness was as low as 0.7 nm in spite of N-rich growth conditions. Typical reflection high-energy electron diffraction (RHEED) patterns for nominally $Sc_{0.18}Al_{0.82}N$/GaN grown at 350 °C, 730 °C, and 890 °C are shown in Fig. 1. At low temperature, the spotty pattern in Fig. 1(a) indicates a 3D growth mode and rougher surface.

Manuscript received July 12, 2017; revised August 25, 2017; accepted August 30, 2017. Date of publication September 6, 2017; date of current version October 27, 2017. This work was supported by the Office of Naval Research. This manuscript contains highlights from the Proceedings of the 2017 International Conference on Compound Semiconductor Manufacturing Technology. *(Corresponding author: Matthew T. Hardy.)*

The authors are with U.S. Naval Research Laboratory, Washington, DC 20375 USA (e-mail: matthew.hardy@nrl.navy.mil).

Color versions of one or more of the figures in this paper are available online at http://ieeexplore.ieee.org.

Digital Object Identifier 10.1109/TSM.2017.2749201

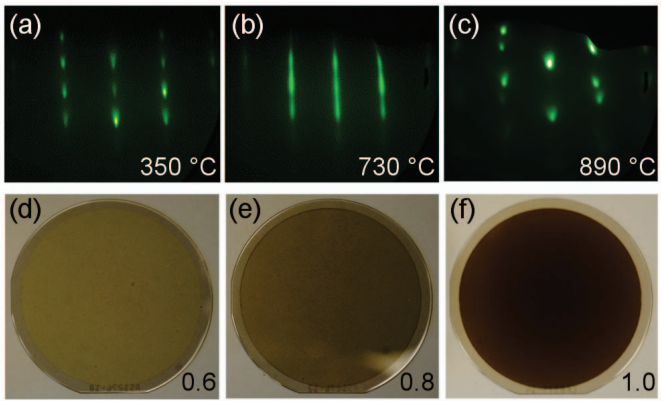

Fig. 1. RHEED images for nominally 80-nm $Sc_{0.18}Al_{0.82}N$-on-GaN samples grown at substrate temperatures of (a) 350 °C, (b) 730 °C, and (c) 890 °C. Wafer images of nominally 200-nm $Sc_{0.18}Al_{0.82}N$ samples grown on 2-in 4H-SiC substrates with III/V ratios of (d) 0.6, (e) 0.8, and (f) 1.0. Note the dark red/orange tint for the film in (f).

In Fig. 1(b) the streaky RHEED pattern indicates a smooth surface and dominate 2D growth mode. At 890 °C, significant Al re-evaporation causes a much higher Sc concentration than expected (x = 0.8), leading to formation of rock-salt ScAlN. The offset first order spots in Fig. 1(c) are consistent with mixed phases or cubic $Sc_xAl_{1-x}N$ grains rotated in-plane.

Plasma-assisted MBE growth of III-N materials typically uses metal-rich growth conditions to improve ad-atom mobility and maintain a smooth, 2D growth mode. In contrast, growth of ScAlN has thus far required N-rich growth conditions. If the total metal (Sc and Al) flux exceeds the active nitrogen flux, X-ray diffraction (XRD) $2\theta/\omega$ scans show additional peaks, attributed to rock-salt $Sc_xAl_{1-x}N$ and $ScAl_x$ intermetallic phases [10]. In addition, the wafer color darkens and takes on a red/orange tint for III/V ratios greater than 1.0, as seen in Fig. 1(f). The tint the III/V $<$ 1 films is attributed to thin film interference. The wafer color likely comes from rock-salt ScAlN inclusions, which have a bandgap in the visible portion of the spectrum, and metallic $ScAl_3$ inclusions.

III. Experimental

$Sc_xAl_{1-x}N$ layers used in this work were grown by RF-plasma assisted MBE using a Scienta-Omicron PRO-75 system. The Al and Ga fluxes were provided by dual-filament effusion cells, and Sc flux was provided by an electron beam evaporator. The Sc flux was controlled during growth using a closed-loop feedback system based on a cross-beam residual gas analyzer, which samples the Sc flux at an angle with respect to the e-beam/sample axis, is compatible with the relatively high N_2 background pressures present during growth, and has the sensitivity to measure relatively low fluxes in real time. The Sc flux was calibrated before each run using a quartz crystal monitor, inserted below the substrate prior to growth. Separately-grown calibration samples were measured *ex-situ* using a combination of energy dispersive X-ray spectroscopy and X-ray photoemission spectroscopy. The $Sc_xAl_{1-x}N$ layers were grown N-rich at a nominal substrate temperature of 700 °C, III/V ratio of 0.8, and growth rate of 3.4 nm/min.

Four samples were grown on 3-in-diameter 4H-SiC substrates for comparative etch rate studies. Two samples were 200-nm-thick $Sc_xAl_{1-x}N$ thin films with x = 0.02 and 0.16. The composition was adjusted by increasing the Sc flux, leading to a small increase in growth rate, but keeping the III/V ratio well within the N-rich regime. In addition, a 600-nm GaN/50-nm AlN sample and 120-nm AlN sample were grown on 4H-SiC to serve as etch rate references. $Sc_{0.02}Al_{0.98}N$ has only 0.24% compressive misfit strain when grown on a relaxed AlN template/substrate, and should have a critical thickness well in excess of 1 μm. Likewise, the $Sc_{0.16}Al_{0.84}N$ sample is near the GaN lattice-matched composition (x = 0.18), where there is no misfit strain [18].

The samples were diced into 1 $\times$ 1 cm^2 squares, patterned with a photoresist etch mask, and co-loaded into an Oxford Instruments Plasmalab 100 ICP system for each $Cl_2/BCl_3/Ar$ ICP etch experiment. The samples were placed on a Si carrier wafer without additional thermal coupling to the carrier. During the etch the carrier was clamped, and the platen temperature was 38 °C, as measured by a thermocouple in contact with the platen backside with no He backside cooling applied. The etch pressure was 5 mTorr, and the process gas flow was $Cl_2/BCl_3/Ar$ at a volumetric flow rate of 20/10/10 sccm, respectively. For the first set of samples, the etch time was varied between 20 s and 150 s and the ICP/bias etch power was held constant at 200/50 W. The two ScAlN samples were excluded from the 20 s etch, due to their low etch depth, and the AlN and GaN samples were excluded from the 150 s etch to avoid etching through the AlN layer. For a second set of samples, the etch time was held constant at 35 s, and the bias power was varied among 30, 50 and 70 W with the ICP power held constant at 200 W. The bias power refers to the RF power applied to the bottom (sample chuck) electrode and directly controls the kinetic energy of ions incident on the wafer surface. The ICP power is the RF power applied to the ICP coil, which influences the process gas ionization and reactivity. The etch depth was measured by profilometry for etch depths greater than 400 Å and by atomic force microscopy (AFM) for the remaining samples. The profilometer and AFM were calibrated using the same calibration standard. Three measurements were made and averaged at each of three locations on each sample.

IV. Results and Discussion

An XRD 0002 rocking curve, AFM micrograph, and RHEED pattern are shown in Fig. 2 for a 200-nm $Sc_{0.19}Al_{0.81}N$ thin film grown on Si-face 4H-SiC under similar conditions as the samples used in the etch study. The XRD rocking curve full-width at half-maximum (FWHM) for the 200-nm film is as low as 1013 arcsec, comparable to GaN layers of similar thickness grown on SiC. The rms surface roughness was as low as 0.64 nm, and RHEED patterns are nearly streaky, showing only slight intensity modulation along the streaks, indicating a smooth surface. Taken together these measurements demonstrate the relatively high quality of epitaxially grown $Sc_xAl_{1-x}N$.

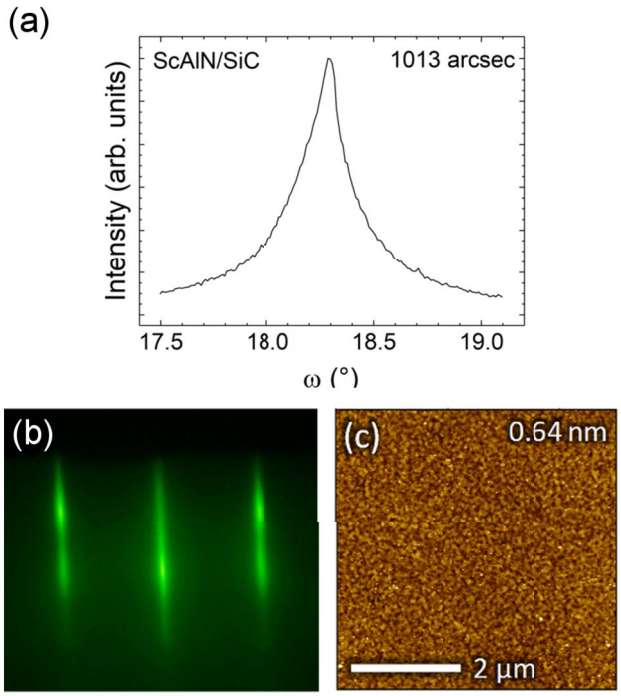

Fig. 2. (a) 0002 reflection XRD rocking curve with FWHM inset, (b) RHEED pattern, and (c) 5 × 5 μm^2 AFM scan with rms roughness inset and a color scale range of 5 nm for a 200-nm $Sc_{0.19}Al_{0.81}N$/4H-SiC sample.

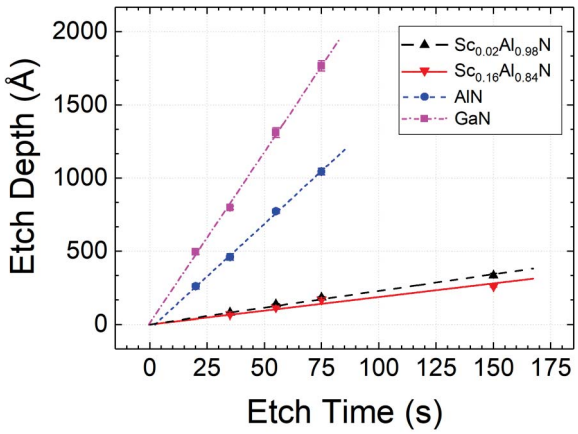

Fig. 3. Measured ICP etch depth for samples co-loaded on a Si carrier wafer with various etch times at ICP/bias powers of 200/50 W.

The measured etch depth versus etch time for the ICP/bias 200/50 W etch conditions is given in Fig. 3. The dead time, given by the x-intercept, is low for each sample, with a maximum of 2.3 s for AlN, indicating the etch is not significantly impacted by surface contamination or oxidation [19]. Error bars are shown corresponding to one standard deviation in etch depth, though in most cases the error bars overlap the data point. For these etch conditions and with only 2% ScN content, the etch selectivity of $Sc_{0.02}Al_{0.98}N$ is 6.7 relative to AlN, and 10.8 relative to GaN. For $Sc_{0.16}Al_{0.84}N$, the selectivity is 9.0 relative to AlN and 14.5 relative to GaN.

The reduction in etch rate for the ScAlN ESL is likely related to the very low vapor pressure of Sc-Cl etch products. Vapor pressure curves for potential III-N etch products

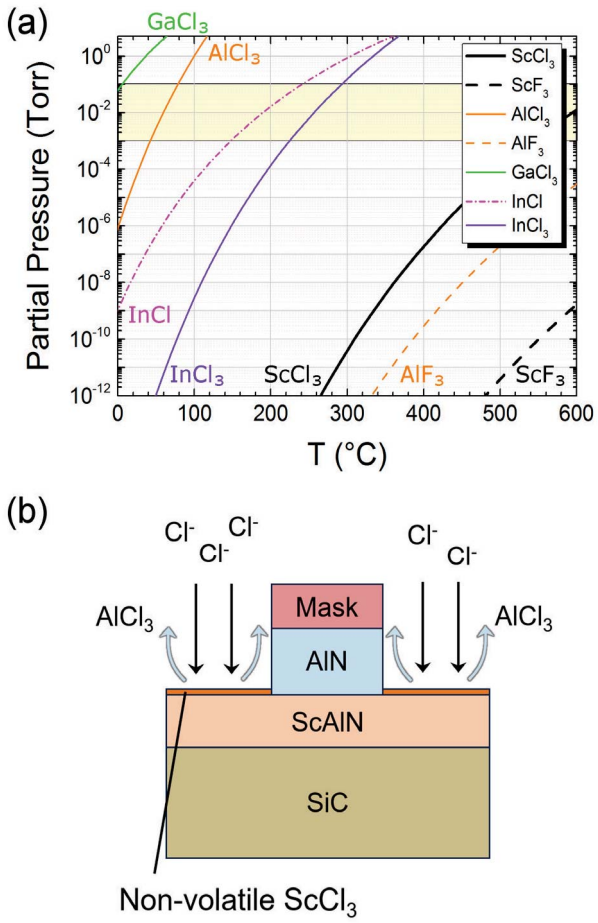

Fig. 4. (a) Vapor pressures of potential ScAlN, AlN, GaN and InN dry etch products when used with chlorine- or fluorine-based etch chemistries [20]. Typical process pressures are highlighted. (b) Schematic depicting etch rate reduction in a ScAlN ESL due to the presence of non-volatile $ScCl_3$ on the etch surface, leading to selectivity with respect to AlN.

are shown in Fig. 4(a). At 50 °C, $ScCl_3$ has a vapor pressure of 3 × 10^{-30} Torr, many orders of magnitude lower than $AlCl_3$ (3 × 10^{-3} Torr) and $GaCl_3$ (2 Torr) [20]. As the ScAlN etch proceeds, $ScCl_3$ etch byproducts accumulate on the surface, while $AlCl_3$ and $GaCl_3$ etch byproducts evaporate. The low vapor pressure of $ScCl_3$ implies a stronger bond with the sample surface and reduced volatility, allowing the $ScCl_3$ etch byproducts to persist on the surface and impede further etching, as shown schematically in Fig. 4(b). Under this model, any change in the etch process which enhances the chemical components of the etch (higher ion and active neutral densities) while leaving the physical components (ion kinetic energy) unchanged or reduced should improve selectivity. Conversely, changes to the etch process which increase the ion kinetic energy (more massive etch species, higher bias power) are expected to reduce the selectivity via sputtering of the rate-limiting $ScCl_3$ layer. The initial ICP etch conditions used here have not been modified from our standard HEMT mesa isolation etch process.

Measured etch rates and etch selectivity relative to AlN are given for varying bias etch power for each sample in Fig. 5. Error bars correspond to one standard deviation, and are dominated by cross-wafer etch depth variation in specific samples.

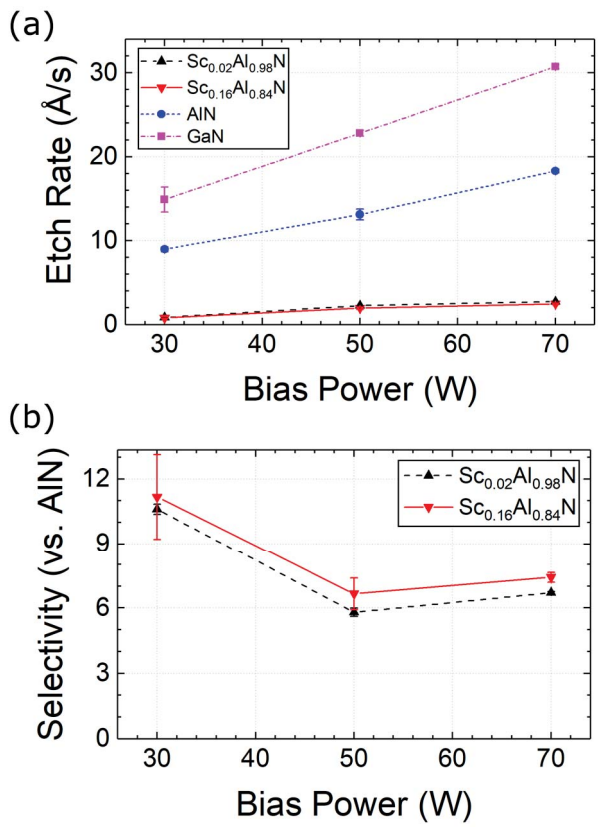

Fig. 5. (a) Etch rate and (b) selectivity relative to AlN for various bias powers with an ICP plasma power of 200 W.

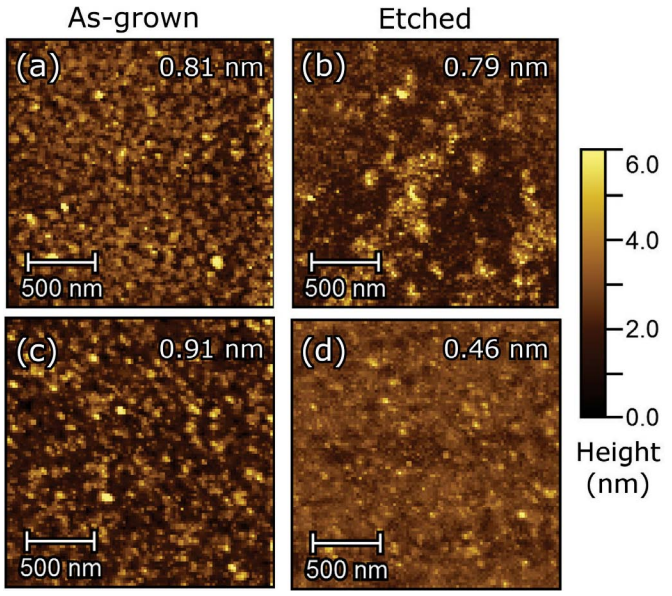

Fig. 6. $2 \times 2\ \mu m^2$ AFM micrographs of an (a) as-grown and (b) etched $Sc_{0.02}Al_{0.98}N$ sample and an (c) as-grown and (d) etched the $Sc_{0.16}Al_{0.84}N$ sample. The rms roughness is inset in each image.

As expected, etch rates increase with bias power for each sample. In addition, the selectivity of the ScAlN samples increases at lower bias power, resulting in a selectivity relative to AlN of 11.2 for $Sc_{0.16}Al_{0.84}N$ and 10.6 for $Sc_{0.02}Al_{0.98}N$. The selectivity relative to GaN is 18.6 and 17.6 for $Sc_{0.16}Al_{0.84}N$ and $Sc_{0.02}Al_{0.98}N$, respectively. The improvement in selectivity at lower bias power is likely related to the reduced kinetic energy of the incoming ions, which are less effective in sputtering the rate-limiting $ScCl_3$ species off the surface. The selectivity does not appear to further decrease for higher bias powers above 50 W, suggesting the ScAlN ESL may be applicable to etch processes that require relatively higher etch rates.

AFM micrographs of as-grown and etched regions of the two $Sc_xAl_{1-x}N$ samples are shown in Fig. 6. The images show the $Sc_{0.02}Al_{0.98}N$ and $Sc_{0.16}Al_{0.84}N$ samples from the etch time series having an etch time of 150 s at 200/50 W ICP/bias power, which resulted in a 304-Å-deep etch for the $Sc_{0.16}Al_{0.84}N$ sample and a 339-Å-deep etch for the $Sc_{0.02}Al_{0.98}N$ sample. There is minimal morphology change after the etch resulting in rms roughness as low as 0.46 nm on the as-etched surface. There are no obvious signs of either pitting [13] or micro-masking [15], although the etch depth may not be sufficient to reveal either process.

In addition to reduced bias power, changing the etch chemistry to reduce the physical component of the dry etch may also help improve selectivity. BCl_3 and Ar do not significantly etch GaN or AlN on their own [19], but they are both relatively high mass species and may contribute significant kinetic energy to the etch process. Other parameters, such as the etch pressure are expected to have a smaller impact on selectivity [13], [14].

Selective etching of ScAlN with respect to AlN using fluorine-based chemistries is unlikely to be successful due to the very low vapor pressure of AlF_3 [20], [21]. However, Sc-containing ESLs used with fluorine etch chemistries have the potential to improve selectivity relative to GaN over existing Al-containing ESLs [13], [16] owing to the vapor pressure of ScF_3, which is significantly lower than AlF_3, as shown in Fig. 4(a). Removal of the ScAlN ESL is of interest for improved process flexibility, and may be possible via modified dry etch chemistries (to maximize the physical component of the etch) or a selective wet etch.

The ability to use a $Sc_xAl_{1-x}N$ ESL compatible with AlN etching or utilizing $Sc_xAl_{1-x}N$ as a lattice-matched ESL for fluorine-free plasma etching of GaN in cases where potential fluorine ion incorporation into the III-N film is undesirable [17] should open up a variety of new or previous impractical applications. Fluorine-chemistry-based plasma etching has been used for HEMTs in the past to etch through various passivation layers prior to gate metallization or for gate recess etching to control threshold voltage [22]–[24]. As shown in Fig. 7, a ScAlN ESL would allow for a post-passivation gate process or improved control of barrier recess etching while avoiding risk of implanting fluorine ions near the active region, which can modify the threshold voltage and degrade mobility [24], [25].

Extraction efficiency can be improved in deep-UV LEDs by removing the AlN substrate, to prevent absorption by defect states [26]. A ScAlN ESL grown below the active region, as shown in Fig. 7(c), could facilitate reproducible substrate removal. Following mounting of the wafer upside-down on a carrier wafer and an initial lapping step, the ScAlN ESL would allow a high power AlN ICP etch to remove

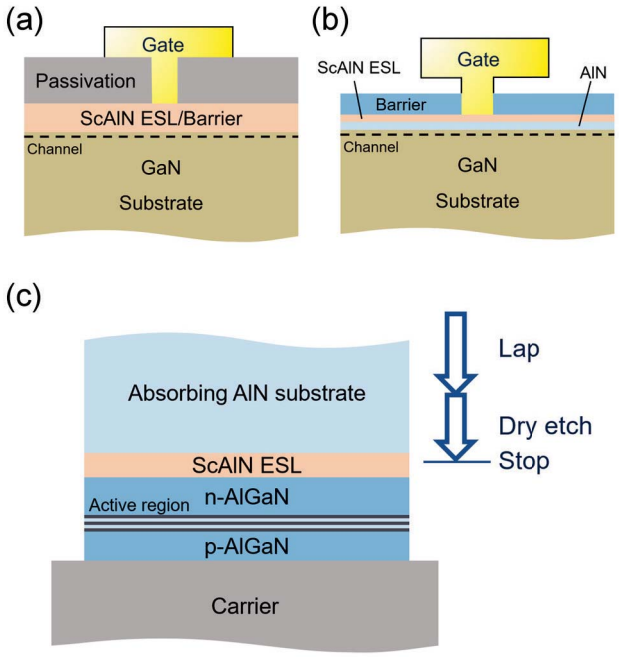

Fig. 7. Schematics showing a ScAlN ESL used in (a) a recess etch in a passivation-first HEMT process, a (b) gate recess etch and (b) an AlN-based deep-UV LED flip-chip substrate removal/micro-cavity LED process.

the remaining AlN substrate without risking over-etching and damaging the LED active region.

Future work will focus on removal of the ESL, either using alternative dry etch or wet etch chemistries. Removal of the ESL will enable down-stream processing without etch rate instabilities resulting from punching through the ESL. In addition, we intend to demonstrate MBE growth of AlN and GaN on ScAlN and demonstrate working devices containing ScAlN ESLs.

V. Conclusion

MBE growth of high-quality, epitaxial $Sc_xAl_{1-x}N$ on 4H-SiC with $x = 0.02$–0.19 has been demonstrated. $Sc_xAl_{1-x}N$ has a reduced etch rate in conventional $Cl_2/BCl_3/Ar$ ICP etching, resulting in selectivity values as high as 11.2 relative to AlN and 18.6 relative to GaN for $x = 0.16$. AFM rms roughness is essentially unchanged after the etch, with rms roughness as low as 0.46 nm, and no evidence of pitting or micro-masking. The demonstrated $Sc_xAl_{1-x}N$ layers can be used as an ESL with minimal misfit strain when grown on either AlN (for $x = 0.02$) or GaN (for $x = 0.16$), and thus little thickness constraint for $Sc_xAl_{1-x}N$ layers grown below, within, or above an epitaxial device layer stack.

References

[1] D. S. Katzer *et al.*, "Epitaxial metallic β-Nb2N films grown by MBE on hexagonal SiC substrates," *Appl. Phys. Exp.*, vol. 8, no. 8, 2015, Art. no. 085501.

[2] X. Li *et al.*, "100-nm thick single-phase wurtzite BAlN films with boron contents over 10%," *Phys. Status Solidi B*, vol. 254, no. 8, 2017, Art. no. 1600699.

[3] M. Akiyama, K. Kano, and A. Teshigahara, "Influence of growth temperature and scandium concentration on piezoelectric response of scandium aluminum nitride alloy thin films," *Appl. Phys. Lett.*, vol. 95, no. 16, 2009, Art. no. 162107.

[4] S. Zhang, D. Holec, W. Y. Fu, C. J. Humphreys, and M. A. Moram, "Tunable optoelectronic and ferroelectric properties in Sc-based III-nitrides," *J. Appl. Phys.*, vol. 114, no. 13, 2013, Art. no. 133510.

[5] M. A. Caro *et al.*, "Piezoelectric coefficients and spontaneous polarization of ScAlN," *J. Phys. Condens. Matter*, vol. 27, no. 24, 2015, Art. no. 245901.

[6] M. A. Moram and S. Zhang, "ScGaN and ScAlN: Emerging nitride materials," *J. Mater. Chem. A*, vol. 2, no. 17, pp. 6042–6050, 2014.

[7] G. Piazza, V. Felmetsger, P. Muralt, R. H. Olsson, III, and R. Ruby, "Piezoelectric aluminum nitride thin films for microelectromechanical systems," *MRS Bull.*, vol. 37, no. 11, pp. 1051–1061, 2012.

[8] M. Moreira, J. Bjurström, I. Katardjev, and V. Yantchev, "Aluminum scandium nitride thin-film bulk acoustic resonators for wide band applications," *Vacuum*, vol. 86, no. 1, pp. 23–26, 2011.

[9] K.-Y. Hashimoto, S. Sato, A. Teshigahara, T. Nakamura, and K. Kano, "High-performance surface acoustic wave resonators in the 1 to 3 GHz range using a ScAlN/6H-SiC structure," *IEEE Trans. Ultrason., Ferroelectr., Freq. Control*, vol. 60, no. 3, pp. 637–642, Mar. 2013.

[10] M. T. Hardy *et al.*, "Epitaxial ScAlN grown by molecular beam epitaxy on GaN and SiC substrates," *Appl. Phys. Lett.*, vol. 110, no. 16, 2017, Art. no. 162104.

[11] H. Sun *et al.*, "Deep-ultraviolet emitting AlGaN multiple quantum well graded-index separate-confinement heterostructures grown by MBE on SiC substrates," *IEEE Photon. J.*, vol. 9, no. 4, pp. 1–9, Aug. 2017.

[12] M. T. Hardy *et al.*, "Epitaxial ScAlN etch-stop layers grown by molecular beam epitaxy for selective etching of AlN and GaN," in *Proc. Int. Conf. Compd. Semicond. Manuf. Technol.*, Indian Wells, CA, USA, 2017, p. 13.2.

[13] D. Buttari *et al.*, "Selective dry etching of GaN over AlGaN in BCl_3/SF_6 mixtures," *Int. J. High Speed Electron. Syst.*, vol. 14, no. 3, pp. 756–761, 2004.

[14] S. A. Smith *et al.*, "High rate and selective etching of GaN, AlGaN, and AlN using an inductively coupled plasma," *Appl. Phys. Lett.*, vol. 71, no. 25, pp. 3631–3633, 1997.

[15] J.-M. Lee, K.-M. Chang, I.-H. Lee, and S.-J. Park, "Highly selective dry etching of III nitrides using an inductively coupled $Cl_2/Ar/O_2$ plasma," *J. Vac. Sci. Technol. B Nanotechnol. Microelectron. Mater. Process. Measu. Phenomena*, vol. 18, no. 3, pp. 1409–1411, 2000.

[16] R. M. Farrell *et al.*, "AlGaN-cladding-free *m*-plane InGaN/GaN laser diodes with p-type AlGaN etch stop layers," *Appl. Phys. Expr.*, vol. 4, no. 9, 2011, Art. no. 092105.

[17] M. T. Hardy, B. P. Downey, and D. J. Meyer, "Scandium-containing III-N etch stop layers for selective etching of III-Ns and related materials," U.S. Patent 62 420 029, 2016.

[18] S. Zhang, W. Y. Fu, D. Holec, C. J. Humphreys, and M. A. Moram, "Elastic constants and critical thicknesses of ScGaN and ScAlN," *J. Appl. Phys.*, vol. 114, no. 24, 2013, Art. no. 243516.

[19] D. Buttari *et al.*, "Origin of etch delay time in Cl_2 dry etching of AlGaN/GaN structures," *Appl. Phys. Lett.*, vol. 83, no. 23, pp. 4779–4781, 2003.

[20] C. L. Yaws, *The Yaws Handbook of Vapor Pressure: Antoine Coefficients*, 2nd ed. Oxford, U.K.: Gulf Professional, 2015.

[21] B. Brunetti, V. Piacente, and P. Scardala, "Vapor pressures of gallium trifluoride, trichloride, and triiodide and their standard sublimation enthalpies," *J. Chem. Eng. Data*, vol. 55, no. 1, pp. 98–102, 2010.

[22] R. Chu *et al.*, "V-gate GaN HEMTs for X-band power applications," *IEEE Electron Device Lett.*, vol. 29, no. 9, pp. 974–976, Sep. 2008.

[23] M. Kanamura *et al.*, "Enhancement-mode GaN MIS-HEMTs with n-GaN/i-AlN/n-GaN triple cap layer and high-*k* gate dielectrics," *IEEE Electron Device Lett.*, vol. 31, no. 3, pp. 189–191, Mar. 2010.

[24] Y. Cai, Y. Zhou, K. M. Lau, and K. J. Chen, "Control of threshold voltage of AlGaN/GaN HEMTs by fluoride-based plasma treatment: From depletion mode to enhancement mode," *IEEE Trans. Electron Devices*, vol. 53, no. 9, pp. 2207–2215, Sep. 2006.

[25] F. Medjdoub *et al.*, "Effect of fluoride plasma treatment on InAlN/GaN HEMTs," *Electron. Lett.*, vol. 44, no. 11, pp. 696–698, May 2008.

[26] R. Collazo *et al.*, "On the origin of the 265nm absorption band in AlN bulk crystals," *Appl. Phys. Lett.*, vol. 100, no. 19, 2012, Art. no. 191914.

Authors' photographs and biographies not available at the time of publication.